Calcium-Mediated Spine Stem Restructuring

D. W. Verzi[1] and S. M. Baer[2]

[1]San Diego State University-Imperial Valley Campus
[2]Arizona State University

Calcium-Mediated Spine Stem Restructuring
by *D. W. Verzi and **S. M. Baer
Running Head: Dendritic Spine Restructuring

Corresponding author:
*D. W. Verzi, Department of Mathematics and Statistics,
San Diego State University-Imperial Valley Campus,
720 Heber Avenue, Calexico CA 92231
Phone: (760)768-5531
Fax: (760)768-5631
Email: verzi@math.sdsu.edu

S. M. Baer, Department of Mathematics and Statistics,
Arizona State University
Tempe AZ 85287

The author wishes to submit final manuscript in AmsTEX.

Abstract: A spine is a protrusion from the dendritic (or somatic) surface of a neuron. In recent experiments, cafffeine-induced calcium released from internal stores was shown to cause elongation of dendritic spine stems in slice cultures. Still another experiment indicates that glutamate-induced increases in calcium may cause spine stem shortening. Harris draws a schematic model to explain these seemingly conflicting results, indicating that a small amount of activity may increase free calcium within the spines and cause spine stem elongation, but an excessive amount of activity may increase intraspine calcium beyond a critical level and cause spine stem shortening (see Fig. 2 in [8]).

This paper develops a mathematical model for a fixed population of spines along the dendrite, each with a dynamic structure and calcium level. The system is integrated over time and space to observe an interdependent relationship between calcium, morphology and chemical/electrical activity. Results of simulation qualitatively capture phenomena observed in recent experiments and exhibit periodic oscillations in potential when the spines have excitable membrane properties by allowing spine structure to transition through threshold geometries for generation of action potentials in a bi-directional manner. As in recent experiments, a variety of chemical and structural profiles emerge, depending on membrane properties, patterns of synaptic input, and initial conditions considered.
Key Words: synapse restructuring, intraspine calcium, dendritic spines

1 Introduction

Experimental evidence is mounting that the physical structure of dendritic spines is modifiable in response to chemical and/or electrical activity [1, 2, 3]. In response to activity, spine head volume (and membrane surface area) can increase or decrease; spine necks can change shape from long and slender to short and stubby, and a single synapse on a single spine head can transform into a spine with multiple heads and multiple synapses [4, 5]. Consequently, populations of spines on dendritic trees are subject to activity-dependent processes.

The mechanisms underlying structural changes in spines may be due to one or more cellular influences. One possible mechanism may be the activation of calcium-dependent enzymes as a result of increased calcium levels at the sites of excitatory synapses [6]. Recent experiments implicate intraspine calcium levels as a mediator for changes in dendritic spine structure [8]. Korkotian and Segal monitored and 3-D reconstructed spines in cultured hippocampal neurons over several hours on a confocal laser scanning microscope. Release of calcium from internal stores in response to pulse applications of caffeine induced a small, transient rise in Ca^{2+} $(200-400\mathrm{n}M)$, but caused a significant increase in the length of spine stems in less than 5 minutes [1]. An opposite response was observed in a similar experiment performed by Halpain, Hippolito and Saffer [7]. They induced a rapid collapse of dendritic spines (also within 5 minutes) by stimulating cultured neurons with glutamate. This caused calcium influx, raising intraspine calcium to much higher levels.

Harris proposes a model for spine stem restructuring based on the above experiments [8]. A primary goal of this paper is to formulate a mathematical description of Harris' model, and to investigate possible interactions between electrical/biochemical activity and structural changes in dendritic spines. The system builds on Wu and Baer's model [9] for a single spine with an activity-dependent stem conductance, and on the cable model [10] to explore how calcium-mediated changes in the structure of a population of spines along a dendrite may influence patterns of electrical activity; and how electrical activity due to synaptic events and excitable membrane dynamics may, over time, influence spine structure and calcium dynamics.

The model qualitatively recovers chemical and morphological phenomena observed in recent experiments and exhibits periodic oscillations in potential when the spines have excitable membrane properties. As in recent experiments, a variety of chemical and structural profiles emerge, depending on membrane properties, patterns of synaptic input, and initial conditions considered. The equations are formulated in Sect. 2 and tested in simulation in Sect. 3, followed by Discussion. A table of parameters, summary of the model, and stability analysis may be found in the Appendix.

2 Methods

Confocal videos from slice culture experiments confirm that activity-dependent processes regulate the structure of the dendrite in hippocampal neurons [8]. A small amount of electrical/chemical activity increases a spine's level of free calcium within the cytosol, and causes the spine stem to elongate. However, a higher level of activity may cause calcium influx and induce spine stem shortening or loss, perhaps due to actin depolymerization [8]. A mathematical description of these observations may be built upon cable theory, a system of partial differential equations which permits the density of spines, membrane potentials, and stem resistance to vary continuously in space and time [10]. Since the length and shape of the spine stem is correlated to its resistance and ultimately to stem current flow, it is of interest to explore how this model for a continuum of spines may be adapted to simulate Harris' model (see Fig. 2 in [8]).

2.1 The Cable Model

The electrical potential $V_d(X,t)$ in a passive dendrite of electrotonic (dimensionless) length $L = l/\lambda$, studded with $\overline{n}$ spines per unit length satisfies the cable equation

$$\tau_m \frac{\partial V_d}{\partial t} = \frac{\partial^2 V_d}{\partial X^2} - V_d + R_\infty \overline{n} I_{ss}, \tag{1}$$

[10] where I_{ss} is the spine stem current, τ_m is the membrane time constant, and R_∞ is the cable input resistance. The fixed spine density ($\overline{n}$) represents the average number of spines per unit length at $X = x/\lambda$. For simulations in this paper, $\lambda = 180\mu m$. (For a detailed derivation of the cable equation, see [10].)

An equation for the membrane potential in each spine head is obtained from a current balance relation for the capacitive, ionic, synaptic and spine stem currents given by

$$C_{sh} \frac{\partial V_{sh}}{\partial t} = -I_{ion} - I_{syn} - I_{ss}. \tag{2}$$

[11]. (See Fig. 1 for the schematic of a single spine.)

The spine stem current is computed as an Ohm's Law voltage drop over the stem resistance:

$$I_{ss} = \frac{V_{sh} - V_d}{R_{ss}} \tag{3}$$

[11].

The term I_{ion} represents the ionic currents passing through the head membrane and I_{syn} the synaptically applied current. In a simulation involving passive spines $I_{ion} = V_{sh}/R_{sh}$, but if the spines have excitable membrane properties, Hodgkin-Huxley kinetics (set to 22^oC) simulate voltage-dependent ion channel currents:

$$I_{ion}(V_{sh}, X, t) = \gamma A_{sh}\big((V_{sh} - V_{Na})\overline{g}_{Na} m^3 h + (V_{sh} - V_K)\overline{g}_K n^4 + (V_{sh} - V_L) g_L\big) \tag{4}$$

[12]. A table of parameters may be found in the Appendix.

Synapses over an interval $X_0 \leq X \leq (X_0 + \Delta X)$ are activated periodically by applying to the spines in that interval

$$I_{syn}(V_{sh}, X, t) = g_{syn}(X,t)(V_{sh} - V_{syn}), \tag{5}$$

where V_{syn} is the synaptic reversal potential and g_{syn} is a brief synaptic conductance generated by the α-function

$$g_{syn}(X,t) = g_p \frac{t}{t_p} e^{(1 - \frac{t}{t_p})}. \tag{6}$$

[11]. In this paper, spines in the interval $0.0 \leq X \leq 2.0$ are activated every $T = 10\text{m}s$.

2.2 Dynamic Morphology

The model now breaks from cable theory [10] to view the spine stem current (I_{ss}) as an important measure, over time (minutes to hours), of the electrical activity between the spine head and dendritic base. The following subsystem, appended to the cable model, explores the possibility that this electrical interaction controls slow, local changes in spine structure and calcium level:

$$\frac{\partial C_a}{\partial t} = \epsilon_1 \big(\eta |I_{ss}| - \rho\big)\big(C_a - C_{min}\big) \tag{7}$$

$$\frac{\partial R_{ss}}{\partial t} = -\epsilon_2 (C_a - C_{crit})(R_{ss} - R_{min})(1 - R_{ss}/R_{max}). \tag{8}$$

Free intraspine calcium (nM) changes proportional to activity (regardless of direction), relative to a minimal level, as measured by $(\eta|I_{ss}| - \rho)$, increasing when $|I_{ss}| > \rho/\eta$ and leaking away slowly when $|I_{ss}| < \rho/\eta$. The ratio of spine stem resistance to input resistance (R_{ss}/R_∞) controls how electrically connected the spine is to the dendrite [10, 11, 5]. In the model, R_∞ is fixed, while R_{ss} varies over time and space, so that the difference between spine head and base potentials $(V_{sh} - V_d)$ becomes negligible as $R_{ss} \to R_{min}$, imposing a kinetic upper bound on calcium (i.e. $|I_{ss}| = |V_{sh} - V_d|/R_{ss}$ becomes small enough so that $\partial C_a/\partial t$ is negative). The factor $(C_a - C_{min})$ prevents calcium from becoming negative in areas receiving no activity over a sustained period of time.

The stem resistance R_{ss} is generally computed as the ratio of the specific cytoplasmic resistance to the cross-sectional area, integrated over the length of the stem [11]. Stem resistance has previously been used as a measure for stem structure [13, 9, 14], since spines with long, narrow stems have a higher resistance to current flow than spines with short, broad stems. Equation (8) models slow, bounded changes in spine structure as measured by stem resistance. Activity-dependent calcium regulates changes in stem resistance, and a critical intraspine calcium level (C_{crit}) controls the direction of change, decreasing for $C_a > C_{crit}$, modelling spine stem shortening, and increasing for $C_a < C_{crit}$, modelling spine stem elongation, as in Harris' model [8].

A low level of synaptic input into spines, over an extended period of time, may increase calcium levels, and the resulting spine stem lengthening may lead synaptic input to depolarize a spine with excitable membrane properties. Threshold conditions for action potential (AP) generation in the spine heads is sensitive to conductance loading provided by the spine stem [11]. Thus, in the model, a fixed density of spines ($\overline{n}$) with little free calcium and below threshold for AP may elongate from a small amount of periodic synaptic input over time and reach threshold for generating an AP (See Fig. 2a-b). The increased stem current from repetitive spiking in each cycle of activity will ramp-up the level of internal free calcium until it passes C_{crit}, and the spine stems begin to shorten over time, as in Fig. 2c-d. When the spine stem no longer provides the necessary conductance loading, APs will cease, and activity will fall below a minimum level $(\eta|I_{ss}| < \rho)$. If periodic synaptic input continues over time at a low level, the calcium will again fall below C_{crit}, and the spine stems will elongate, repeating the cycle of morphological adaptation. Thus, for spines with excitable membrane, the model can exhibit burst oscillations between periods of active and silent phases, allowing calcium to modulate signaling within the dendritic tree. A summary of the fast and slow system, including initial and boundary conditions, along with a table of parameters may be found in the Appendix.

3 Results

Of initial interest is how the above system may affect local activity and structure for spines with passive membrane properties. Figure 3 compares the results for two separate simulations of 63 spines, located uniformly along a dendrite of electrotonic length $L = 3$ ($\overline{n} = 21$ spines/$e.l.$), for two different levels of synaptic activity. The spines at $0.0 \le X \le 0.2$ are activated every 10ms with I_{syn} (Eq. (5)-(6)), with peak synaptic input (g_p from Eq. (6)) occuring at $t_p = 0.2$ms in each activation cycle. Since the spine head membrane is considered to be passive, $I_{ion} = V_{sh}/R_{sh}$.

For the first simulation, calcium and stem resistance are initially uniform at $C_a = 800\text{n}M$ (above $C_{crit} = 300\text{n}M$) and $R_{ss} = 1600\text{M}\Omega$, respectively. Peak synaptic activation reaches $g_p = 0.074\text{n}S$ in each cycle, modelling a weaker synapse. Figure 3 (left), shows a time course for head potential, intraspine calcium and stem resistance for the spines under synaptic activation at $X = 0.0$ over 50 activation cycles. Calcium decreases throughout the simulation (approaching $C_{min} = 0.0$), since the stem current is less than ρ/η. When $C_a > C_{crit}$, during the first 15 cycles, R_{ss} decreases to a minimum of $950\text{M}\Omega$, modelling spine stem shortening, and then increases during the remaining 35 cycles (approaching $R_{max} = 1800\text{M}\Omega$) when $C_a < C_{crit}$, modelling spine stem elongation (Fig. 3b-c). In Fig. 3a, the maximum amplitude for V_{sh} in each cycle of activation is proportional to R_{ss}, since current flows more rapidly from spines when stem resistance is low.

For the second simulation, calcium and stem resistance are initially uniform at $C_a = 200\text{n}M$ (below $C_{crit} = 300\text{n}M$) and $R_{ss} = 1000\text{M}\Omega$, respectively, and $g_p = 0.37\text{n}S$, modelling a higher level of synaptic activity. Figure 3 (right) again shows a time course for head potential, intraspine calcium and stem resistance for spines under synaptic activation over 50 applications of I_{syn}. Now calcium increases throughout the simulation, reaching a critical level after 25 activations. Now stem resistance increases until C_a crosses C_{crit} from below, and then decreases for the remainder of the simulation.

3.1 Spines with Excitable Membrane Properties

Since 90% of excitatory synapses terminate on dendritic spines [4], this section explores the effects that calcium-mediated dynamic morphology may have upon the generation and propagation of APs when the spines have excitable membrane properties. In the next simulation, average spine density is fixed uniformly at $\overline{n} = 21$ excitable spines/ $e.l.$, with initial uniform values of $R_{ss} = 800\text{M}\Omega$ and $C_a = 100\text{n}M$. Spines are synaptically activated every $10\text{m}s$ with a weaker input as in the second passive simulation ($g_p = 0.074\text{n}S$), but now the spines can generate and propagate an AP when properly stimulated, using Hodgkin-Huxley kinetics [12] to model ionic current in the spine heads (Eq. (4)). Figure 4 graphs a time course for 150 activation cycles for head potential, calcium and stem resistance under synaptic input.

For a fixed density of spines, an excitable response depends on the stem resistance [11], now a dynamic variable. The initial value for R_{ss} is below threshold to generate an AP for 21 spines/$e.l.$, so that peak head potential is less than $20\text{m}V$ for the first 10 cycles of activation (Fig. 4a). Calcium is initially less than C_{crit} and decreases during this "silent" phase (absence of APs), so that resistance increases (stems elongate) at $X = 0.0$ (Fig. 4b-c). When stem resistance reaches a threshold value of approximately $1000\text{M}\Omega$, the spines begin firing APs, causing calcium to increase. Stem resistance and peak values for head potential and stem resistance continue to rise, until $C_a = C_{crit}$. The "active" phase of repetitive spiking in head potential continues until $t = 800\text{m}s$, as resistance slowly decreases (stems shorten), for calcium above a critical level. Calcium reaches a peak value of $820\text{n}M$ just before activity begins a second silent phase. Then calcium and resistance decrease until $C_a < C_{crit}$ again at $t = 1000\text{m}s$.

The results from Fig. 4 raise several questions: Will the bursting pattern for active and silent phases continue over time, and what effect does this pattern of impulses have upon the spines "downstream" from the stimulated region. Figure 5 compares results under synaptic activation and downstream for 500 cycles of activation for the same simulation shown in Fig. 4. Figures 5a and 5b graph head and dendritic potentials over time at $X = 0.0$ (left) and $X = 1.0$ (right). Figure 5c shows a state space diagram for the slow variables of calcium and resistance over the same period of time at these same locations.

Let us first consider what is happening in the stimulated region ($X = 0.0$ left). In Fig. 5a, the initial resistance is just below threshold for generation of APs, so that $\eta|I_{ss}| < \rho$ and calcium decreases while R_{ss} increases since $C_a < C_{crit}$ (Quadrant 1 Fig. 5c)until spines in the stimulated region begin firing APs.

Since $\eta|I_{ss}| > \rho$ (on average over each activation cycle) in the presence of APs, both measured quantities continue to rise (Quadrant 2) until $C_a = C_{crit}$ and R_{ss} is approximately 1770MΩ. Spiking continues while C_a increases and R_{ss} decreases (Quadrant 3) until stem resistance once again falls below threshold for AP generation (approximately 1000MΩ) and C_a reaches its peak value of approximately 820nM after 80 cycles of activation (c.p. Fig. 5c to Fig. 4b). A silent phase then begins in the absence of AP generation, as both measured quantities decrease (Quadrant 4) until $C_a = C_{crit}$ and R_{ss} is approximately 570MΩ. Once $C_a < C_{crit}$, resistance begins rising toward threshold, and a period of high level activity begins again after 120 applications of I_{syn} (Fig. 5a). The potential in the dendrite at the base of the spines (V_d) is graphed in Fig. 5b to compare differences from $X = 0.0$ to 1.0.

Downstream from synaptic activation, at $X = 1.0$, there are several noticeable differences in the graphs. The shapes of the active and silent phases are different, the magnitude for potential during silent phases is much smaller in both the spines and the dendrite, and the phase plane indicates that (C_a, R_{ss}) is tending to $(0.0, R_{max})$. While the spines downstream are brought to threshold by APs firing in the stimulated region, the edges of the active phases are sharper (c.p. left), an indication of the "all or nothing response" that occurs in the absence of synaptic input; i.e. spines at $X = 0.0$ have a few cycles where they are generating APs just below threshold for propagation on the leading and trailing edges of each active phase. Potentials in both the spines and the dendrite are greatly reduced during silent phases (c.p. left) since current flowing down the dendrite is attenuated by increasing values for R_{ss}. At the end of the initial silent phase, resistance at $X = 1.0$ is approximately 1200MΩ, but approaches R_{max} by the end of the second silent phase (Fig. 5c right).

Calcium is initially less than C_{crit}, and decreases throughout the simulation, causing R_{ss} to increase toward its upper bound, further isolating the spines downstream and locally reducing $|I_{ss}|$. There are brief periods of time in each AP response when C_a increases slightly (note the "noise" in Fig. 5c), but on average, calcium decreases and resistance increases over each 10ms-cycle, so that $(C_a, R_{ss}) \rightarrow (0.0, R_{max})$ at $X = 1.0$. A stability analysis for critical points in the slow subsystem is included in the Appendix.

4 Discussion

This paper considers one way to model the interdependence of activity and morphology in the dendrite by theoretically studying specifically observed phenomena. Intraspine calcium levels respond to local changes in activity and mediate spine structure, as measured by stem resistance. The model qualitatively captures chemical and morphological phenomena observed in recent experiments. Intraspine calcium levels decrease in response to weaker synaptic activation ($g_p = 0.074$nS) and increase in response to stronger synpatic inputs ($g_p = 0.37$nS) or AP generation in the spine heads. Stem resistance increases (modelling stem elongation) when calcium is subcritical, and decreases (modelling stem shortening) when calcium is supercritical.

The model predicts a higher percentage of spines more electrically connected to the dendrite (shorter spine stems) in areas receiving a sustained high level of activity. Results also predict that areas of the dendrite experiencing a sustained lack of electrical activity (whether synaptic activation or current flowing along the dendrite) will have a higher percentage of spines with long, narrow stems. The result that stem resistance increases monotonically outside the stimulated region (see Fig. 5c) is consistent with experimental observations that dendrites are more spiny when synapses are inactivated, possibly to compensate for lost activity [15]. The length of time for chemical and structural transition depends on the magnitudes of ϵ_1 and ϵ_2, respectively, selected here for computational efficiency. To achieve the changes shown in this paper over 5-10 minutes, as observed in recent experiments [1, 7], one would need to set the rates of change in calcium and resistance to 10^{-5}, and 10^{-6}, respectively (three orders of magnitude lower than values used for this

paper.)

By allowing the morphology of the dendrite to transition through identified threshold geometries for generating an AP, new pathways are created for wave propagation when the spines are modelled with excitable membrane properties. Results shown here are for a dendrite of physical length 3λ, where λ is approximately $180\mu m$. This means that the signal propagation to $X = 1.0$ shown in Fig. 5 represents a wave of APs extending to a physical length of $x = 0.18\mathrm{m}m$, resulting from synaptic activation (I_{syn}) of 5 synapses located between $x = 0.0$ and $0.036\mathrm{m}m$, along with the evolving structural profile from previous synaptic events.

In this paper, η and ρ were selected so $\eta|I_{ss}| - \rho$ was negative for passive spines receiving low levels of synaptic input, and positive for passive spines receiving higher levels of activation (using g_p as a measure of magnitude). Using the same values for η and ρ and the lower value for g_p, the model can create and then dissolve a path for impulse propagation when the spines have excitable membrane properties, by allowing stem resistance for activated spines to transition through identified threshold values for generating an AP. For spines with excitable membrane properties, $\eta|I_{ss}| - \rho$ is positive in the presence of low-level synaptic input and membrane response APs, and negative in the absence of either of these two quantities.

The interdependent changes in activity and structure presented here kinetically limit the time period for sustained higher levels of activity, and prevent calcium from reaching a toxic level for the neuron. Shortening the stems causes spines to become more electrically connected to the dendrite, thereby reducing activity and calcium levels in an isolated compartment of the cell. Restructuring neural circuitry modulates signaling, and may also serve as a mechanism to prevent necrosis.

The simple proportional relationship between calcium and activity, presented here as a first step in the modelling process, cannot capture all of the dynamic processes involved in a system with activity-dependent morphology. Nevertheless, the strength of this model is that, like the experimental studies, it helps to dissect the complex phenomenon of these processes. Using a continuum model allows us to exhibit a variety of morphologies and membrane properties with just a few differential equations. The equation for ionic current (Eq. (4)) could include voltage-dependent calcium currents, or the formulation could include a spatio-temporal profile for Ca^{2+} in the spines and the dendritic shaft, addressing calcium diffusion and the influx of calcium through spine stems. Since the region for synaptic input was constant in this paper, it would be interesting to consider simulations where the activation site is randomly selected in each cycle.

ACKNOWLEDGMENTS

DWV was supported by NSF DBI-9602226: Research Training Grant-Nonlinear Dynamics in Biology, awarded to the University of California, Davis; and Faculty Grant-in-Aid 242122 from San Diego State University. SMB was supported by NSF DMS-9320597. The authors gratefully acknowledge M. B. Rheuben of Michigan State University for helpful discussions, and Armando Solorzano of El Centro, CA for graphics.

References

[1] Korkortian, E; Segal, M (1999) Release of calcium from stores alters the morphology of dendritic spines in cultured hippocampal neurons. *Proc. Natl. Acad. Sci.* **96**, 12068-12072.

[2] Maletic-Savatic, M; Malinow, R; Svoboda, K (1999) Rapid dendritic morphogenesis in CA1 hippocampal dendrites induced by synaptic activity. *Science* **283**, 1923-1927.

[3] Segev, I; Rall, W (1998) Excitable dendrites and spines: Earlier theoretical insights elucidate recent direct observations. *Trends Neurosci.* **21**, 453-460.

[4] Harris, KM (1999) Structure, development, and plasticity of dendritic spines. *Curr. Opin. Neurobiol.* **9**, 343-348.

[5] Shepherd, GM (1996) The dendritic spine: A multifunctional integrative unit. *J. Neurophysiol.* **75**, 2197-2210.

[6] Horner, CH (1993) Plasticity of the dendritic spine. *Prog. Neurobiol.* **41**, 281-321.

[7] Halpain, S; Hipolito, A; Saffer, L (1998) Regulation of F-actin stability in dendritic spines by glutamate receptors and calcineurin. *J. Neurosci.* **18**, 9835-9844.

[8] Harris, KM (1999) Calcium from internal stores modifies dendritic spine shape. *Proc. Natl. Acad. Sci.* **96**, 12213-12215.

[9] Wu, HY; Baer, SM (1998) Analysis of an excitable dendritic spine with an activity-dependent stem conductance. *J. Math. Biol.* **36**, 569-592.

[10] Baer, SM; Rinzel, J (1991) Propagation of dendritic spikes mediated by excitable spines: A continuum theory. *J. Neurophysiol.* **65**, 874-890.

[11] Segev, I; Rall, W (1988) Computational study of an excitable dendritic spine. *J. Neurophysiol.* **60**, 499-523.

[12] Hodgkin, A; Huxley, A (1952) A quantitative description of membrane current and its application to conduction and excitation in nerve. *J. Physiol.* (Lond.) **117**, 500-544.

[13] Kuske, R; Baer, SM (2002) Asymptotic analysis of noise sensitivity in a neuronal burster. *B. Math. Biol.* **64**, 447-481.

[14] Verzi, DW (2003) Modelling activity-dependent synapse restructuring. Accepted *B. Math. Biol.* October, 2003.

[15] Kirov SA; Harris KM, (2000) Dendrites are more spiny on mature hipppocampal neurons when synapses are inactivated. *Nat. Neur.* **2**(10) 878-83.

[16] Waltman, P *A Second Course in Elementary Differential Equations* (Academic Press, Inc. Orlando, 1986).

5 Appendix

5.1 Table of Parameters

R_i	specific cytoplasmic resistivity	$70\Omega \cdot cm$
R_m	passive membrane resistance	$2500\Omega \cdot cm^2$
C_m	specific membrane capacitance	$1\mu F cm^2$
R_∞	input resistance	$R_m/(\lambda \pi d)$
λ	length constant	$\sqrt{R_m d/4R_i}$
τ_m	membrane time constant	$R_m C_m$
d	diameter of the dendrite	$0.36\mu m$
A_{sh}	surface area of each spine head	$1.31\mu m^2$
C_{sh}	capacitance of each spine head	$A_{sh} C_m$
γ	channel density	2.5
V_{Na}	sodium reversal potential	$115\text{m}V$
V_K	potassium reversal potential	-12mV
V_L	leakage reversal potential	$10.5989\text{m}V$
V_{syn}	synaptic reversal potential	$100\text{m}V$
$\overline{g}_{Na}$	maximal sodium conductance	$120\text{m}S/cm^2$
$\overline{g}_K$	maximal potassium conductance	$36\text{m}S/cm^2$
$\overline{g}_L$	maximal leakage conductance	$0.3\text{m}S/cm^2$
g_p	peak synaptic conductance	(see figure legends)
t_p	time to peak in each activation cycle	$0.2\text{m}s$
T	time between synaptic activations	$10\text{m}s$
R_∞	input resistance of the dendrite	$1233\text{M}\Omega$
R_{sh}	resistance of each spine head	$1.02\text{x}10^{11}\Omega$
R_{max}	stem resistance upper bound	$1800\text{M}\Omega$
R_{min}	stem resistance lower bound	$500\text{M}\Omega$
ϵ_1	rate of change in calcium	0.01
ϵ_2	rate of change in stem resistance	0.001
C_{crit}	critical intraspine calcium level	$300\text{n}M$
ρ	measure of minimal local activity	1.0
η	scaling parameter for stem current	$1.0\text{x}10^9$

5.2 Summary of Equations

$$\tau_m \frac{\partial V_d}{\partial t} = \frac{\partial^2 V_d}{\partial X^2} - V_d + R_\infty \overline{n} I_{ss} \tag{9}$$

$$C_{sh} \frac{\partial V_{sh}}{\partial t} = -I_{ion} - I_{syn} - I_{ss} \tag{10}$$

$$\frac{\partial C_a}{\partial t} = \epsilon_1 C_a \big(\eta |I_{ss}| - \rho\big) \tag{11}$$

$$\frac{\partial R_{ss}}{\partial t} = -\epsilon_2 (C_a - C_{crit})(R_{ss} - R_{min})(1 - R_{ss}/R_{max}). \tag{12}$$

Calcium is bounded below by $C_{min} = 0.0$, with a critical intraspine calcium level, $C_{crit} = 300\text{n}M$. Spine stem structure is modelled by R_{ss}, increasing for $C_a < C_{crit}$ and decreasing otherwise. Stem resistance is bounded between $R_{min} = 500\text{M}\Omega$ and $R_{max} = 1800\text{M}\Omega$. The density of spines per unit length ($\overline{n}$) is fixed over time, but may vary in X. Both ends of the dendrite are sealed, so that the voltage gradient is always zero at the boundaries, with a resting potential of zero in the dendritic shaft and the spines, i.e.

$$\frac{\partial V_d}{\partial t}(0,t) = 0.0 \tag{13}$$

$$\frac{\partial V_d}{\partial t}(L,t) = 0.0 \tag{14}$$

$$V_{sh}(X,0) = 0.0 \tag{15}$$

$$V_d(X,0) = 0.0. \tag{16}$$

If the spines are passive, then $I_{ion} = V_{sh}/R_{sh}$, but if the spines have excitable membrane properties, the ionic current is modelled using Hodgkin-Huxley kinetics [12]

$$I_{ion}(V_{sh}, X, t) = \gamma A_{sh} \big((V_{sh} - V_{Na}) \overline{g}_{Na} m^3 h + (V_{sh} - V_K) \overline{g}_K n^4 + (V_{sh} - V_L) g_L \big) \tag{17}$$

with increased channel densities [10]. Synaptic input is simulated by applying

$$I_{syn}(V_{sh}, X, t) = g_p \frac{t}{t_p} e^{(1 - \frac{t}{t_p})} (V_{sh} - V_{syn}) \tag{18}$$

every 10ms. The system comes to full rest between activations, since synaptic input reaches its maximum value at $t_p = 0.2$ms.

Equations are integrated using a semi-implicit Crank-Nicholson/Adams-Bashforth finite differencing method, verified against a fully explicit method. For stability, $\Delta X = .04$ and $\Delta t = .005$. Since a significant change in spine structure has been observed over minutes to hours and individual APs are on a time scale of milliseconds (ms), the computation time for a simulation could be on the order of hours. To identify values for $\epsilon_i << 1$ $(i = 1, 2)$ that reduce computation time, but preserve the basic dynamics of the system as $\epsilon_i \to 0.0$, results were compared during corresponding cycles for different simulations, varying ϵ_i. For example, results for the time course of a propagating wave of APs over 60 cycles of synaptic events using ϵ_i are superimposed over results of every other cycle from a second simulation, using $\epsilon_i/2$. As ϵ_i is successively reduced, the animations converge, and ϵ_i is chosen to be computationally efficient, yet sufficiently small to preserve the qualitative structure of results for longer time periods as $\epsilon_i \to 0.0$.

5.3 Stability Analysis for the Slow Variables

The equations for change in calcium and resistance constitute a slow subsystem. Fixing X at one point along the dendrite, insight may be obtained into the stability of stationary points at that location by considering the average contribution of the fast variables to the measure for change in the slow system over each cycle of length T:

$$|V_{sh} - V_d|^{avg} = \frac{1}{T} \int_{T_{i-1}}^{T_i} |V_{sh} - Vd| dt. \tag{19}$$

Numerical simulations indicate that $|V_{sh} - V_d|^{avg}$ is approximately piecewise constant for a fixed location X, with c_1 representing the value for active phases of bursting, and c_2 the value during silent phases. Further, the response of the system over the synaptically activated region behaves as though it were space-clamped; i.e., the state variables are independent of X in that region. Thus one may average over the fast variables

(activity) since the slow variables (C_a and R_{ss}) are relatively constant within activation cycles. In general, c_1 and c_2 are different, but insights into the dynamics of the slow system may be obtained by setting $c_1 = c_2$ and averaging over the fast system to obtain the following ordinary differential equations for dynamic morphology:

$$\frac{dC_a}{dT} = \epsilon_1\big(\eta\frac{|V_{sh} - V_d|^{avg}}{R_{ss}} - \rho\big)(C_a - C_{min}) \tag{20}$$

$$\frac{dR_{ss}}{dT} = -\epsilon_2(C_a - C_{crit})(R_{ss} - R_{min})(1 - R_{ss}/R_{max}). \tag{21}$$

This system has critical points at $\big(C_a^*,\ R_{ss}^*\big) = \big(C_{crit},\ \frac{\eta|V_{sh}-V_d|^{avg}}{\rho}\big)$, $(C_{min},\ R_{max})$ and $(C_{min},\ R_{min})$. To first order, the stability of these points in the non-linear system is related to the eigenvalues of the operator matrix (Jacobian) for the corresponding linearized system, evaluated at the fixed points [16]. The generalized Jacobian for the above system is

$$\begin{bmatrix} \epsilon_1\big(\frac{\eta|V_{sh}-V_d|^{avg}}{R_{ss}^*} - \rho\big) & -\frac{\epsilon_1(C_a^*-C_{min})|V_{sh}-V_d|^{avg}}{R_{ss}^*} \\ -\frac{\epsilon_2}{R_{max}}\big(R_{ss}^* - R_{min}\big)\big(R_{max} - R_{ss}^*\big) & -\frac{\epsilon_2}{R_{max}}(C_a^* - C_{crit})(R_{max} + R_{min} - 2R_{ss}^*) \end{bmatrix}. \tag{22}$$

Evaluating the Jacobian at the point $\big(C_a^*,\ R_{ss}^*\big) = \big(C_{crit},\ \frac{\eta|V_{sh}-V_d|^{avg}}{\rho}\big)$, yields

$$\begin{bmatrix} 0 & -\frac{\epsilon_1\rho^2(C_{crit}-C_{min})}{\eta^2|V_{sh}-V_d|^{avg}} \\ -\frac{\epsilon_2}{R_{max}}\big(R_{ss}^* - R_{min}\big)\big(R_{max} - R_{ss}^*\big) & 0 \end{bmatrix}. \tag{23}$$

The trace of the matrix is zero and the determinant is negative, so that the eigenvalues are real and of opposite sign. Since one eigenvalue is positive, independendent of the location along the dendrite, this critical point is unstable in the linear system, and, therefore, unstable at each location X in the nonlinear system [16].

For the second fixed point, $(C_{min},\ R_{max})$, the Jacobian is

$$\begin{bmatrix} \epsilon_1\big(\frac{\eta|V_{sh}-V_d|^{avg}}{R_{max}} - \rho\big) & 0 \\ 0 & -\frac{\epsilon_2}{R_{max}}(C_{min} - C_{crit})(R_{min} - R_{max}) \end{bmatrix}, \tag{24}$$

with eigenvalues along the diagonal. The sign of (a_{22}) is always negative since $C_{min} < C_{crit}$ and $R_{min} < R_{max}$, but the sign of the (a_{11}) depends on the level of local activity when $R_{ss} = R_{max}$. Excitable spines at $0.0 \leq X \leq 0.2$ are spiking in response to synaptic activation when $R_{ss} = R_{max}$, so that $(a_{11}) > 0$ in the presence of local synaptic activation and AP generation. Therefore, the fixed point is unstable for synaptically activated spines. However, spines downstream are spiking in response to activity flowing along the dendrite so that the difference in local head and dendritic potentials is, on average, smaller in the absence of synaptic activation. For spines downstream, $\eta|V_{sh} - V_d|^{avg} < \rho/R_{max}$, for parameter values in this paper. Therefore, $(a_{11}) < 0.0$ and the fixed point is stable.

A similar analysis for the remaining critical point indicates that (C_{min}, R_{min}) also has eigenvalues along the diagonal with (a_{11}) as above, but $(a_{22}) = -\epsilon_2(C_{min} - C_{crit})(R_{max} - R_{min})/R_{max} > 0.0$, since $R_{max} > R_{min}$. The Jacobian has at least one positive eigenvalue, independent of location along the dendrite, and this point is always unstable.

In summary, with the above assumptions at each location X under synaptic activation, the system has no stable fixed points in a bounded region of the plane, since $R_{min} \leq R_{ss} \leq R_{max}$, $C_{min} \leq C_a$, and calcium is kinetically bounded above by the periodic behavior of activity, for the chosen parameter values. Removing the unstable point $(C_a^*,\ R_{ss}^*)$ inside this region permits application of the Poincare-Bendixson theorem (Waltman, 1986) to conclude that trajectories in this region would be either periodic, or have an omega limit set that is periodic.

In Fig. 6, three results are plotted for the same simulation as in Fig. 5 (smoothing the trajectories for comparison) with different initial conditions for calcium and resistance. The outer two trajectories were run for 500 activation cycles, and the inner trajectory (dashed) was run for 1200 cycles. Since, in general, $c_1 \neq c_2$ in Eq. (7)-(8), the trajectories are not exactly periodic over time. Fixing X at a point not under synaptic activation, the above system has only one stable fixed point. Unless the system is started exactly at one of

the other two critical points, trajectories will tend to $(C_{min},\ R_{max})$ over time (see Fig. 5c right).

Fig. 1 Schematic diagram of a single dendritic spine. A spine is a protrusion from the dendritic (or somatic) surface of a neuron. Dimensions vary, with typical ranges that include stem lengths of order 1.0μm, diameters of order 0.1μm and head surface areas of order 1.0μm^2. I_{syn} denotes input current into the spine head. Spines may be modelled with passive or excitable membrane properties by varying the formulation for I_{ion}. In this paper, the magnitude of the stem current ($|I_{ss}| = |V_{sh} - V_d|/R_{ss}$) measures local activity (regardless of direction), and stem resistance (R_{ss}) measures spine structure, decreasing (to model stem shortening) when calcium is above a critical value, and increasing (to model stem elongation) when calcium is below that value.

Fig. 2 Morphological adaptation allows the spines to respond to, and regulate levels of local activity. Spine stem structure is related to the amount of free calcium present in the spines, and changes in calcium levels are proportional to the amount of local activity. **(a)** A small amount of synaptic activity may raise calcium levels slightly, causing spine stems to elongate, and stem resistance (R_{ss}) to increase. **(b)** If synaptic activity persists over time, calcium may continue to increase beyond a critical amount. **(c)** If the spines have excitable membrane properties, increased stem length (resistance) may depolarize the spine head beyond threshold for generation of an AP. **(d)** In any case, increased levels of synaptic activity, or AP responses increase calcium beyond a critical level for the spines, and stems begin to shorten, lowering stem resistance. **(e)** Stems may be partially or completely retracted into the dendrite, so that synaptic input is no longer directed at an isolated compartment, reducing local activity and calcium levels. When stem resistance falls below threshold for depolarizing excitable spines, AP generation ceases, lowering the level of activity and decreasing the amount of calcium present. If low-level activity continues, over time, calcium will increase and stems will elongate, to enter another cycle of morphological adaptation.

Fig. 3 Intraspine calcium levels depend on activity, and mediate structural change. Sixty-three spines with passive membrane properties are located uniformly along a dendrite of electrotonic length $L = 3$. Spines over $0.0 \leq X \leq 0.2$ are synaptically activated every 10ms with Eq. (5)-(6), for two separate simulations. Time courses are shown for head potential, free intraspine calcium and stem resistance over 50 cycles of activation at $X = 0.0$. Graphs on the left show results for a simulation with peak synaptic activation (g_p) reaching 0.074nS in each cycle, and initial values for calcium and stem resistance uniformly set to $C_a = 800\text{n}M$ (above C_{crit}) and $R_{ss} = 1600\text{M}\Omega$, respectively. Graphs on the right are for a simulation with g_p reaching 0.37nS in each cycle, and initial values for calcium and stem resistance uniformly set to $C_a = 200\text{n}M$ (below C_{crit}) and $R_{ss} = 1000\text{M}\Omega$, respectively. **(a)** Maximum values for V_{sh} in each cycle are proportional to g_p, and also to R_{ss}, since current flows out of stimulated spines more rapidly when resistance is low. **(b)** Calcium decreases toward a lower bound ($C_{min} = 0.0$) when $\eta|I_{ss}| - \rho < 0.0$ (left) and increases when $\eta|I_{ss}| - \rho > 0.0$ (right). **(c)** Stem resistance decreases when $C_a > C_{crit}$, and increases when calcium is subcritical.

Fig. 4 Calcium mediates bidirectional changes in structure and activity when the spines have excitable membrane properties. Sixty-three excitable spines are uniformly located along a dendrite of electrotonic length $L = 3$. Ionic current in the spine heads is modelled with Eq. (4)). Initial values are uniformly $C_a = 100\text{n}M$ and $R_{ss} = 800\text{M}\Omega$ (below threshold for $\overline{n} = 21$ spines per unit length). Spines are synaptically activated with a low level of input as in Fig. 3 (right) ($g_p = 0.074\text{n}S$), and time courses are shown for head potential, free calcium and stem resistance over 150 activation cycles at $X = 0.0$. **(a)** Potential is proportional to stem resistance, initially low for 10 synaptic acivations (c.p. to Fig. 3). An active phase of 80 APs begins when stem resistance for spines in the stimulated region crosses threshold for AP generation (in (c)). A silent phase of 40 cycles (400ms) begins when R_{ss} falls below threshold. **(b)** Calcium decreases during silent phases in head potential, and increases to a maximum of 820nM after 90 cycles of synaptic input when spiking terminates. Calcium returns to a minimum of 50nM over the following 400ms, before increasing again when spiking returns to the spines under synaptic activation. **(c)** Stem resistance increases for 52 cycles of synaptic input when $C_a < C_{crit}$, asymptotically approaching $R_{max} = 1800\text{M}\Omega$. Stem resistance decreases for the next 60 cycles when $C_a > C_{crit}$, reaching a minimum value of 580MΩ after 112 cycles, before beginning to rise again.

Fig. 5 A cycle for structural change induces periodic spiking in spines with excitable membrane properties. Time series for head and dendritic potential are shown over 500 activation cycles (in (a) and (b), respectively), along with a state space diagram for calcium and stem resistance (in (c)) at two different locations, for the same simulation in Fig. 4 ($g_p = 0.074\text{n}S$). Results are shown for $X = 0.0$, under synaptic activation (left), and for $X = 1.0$, downstream (right). **(a)** Alternating periods of active and silent phases in AP generation and propagation occur over time as R_{ss} increases and decreases through threshold values. The magnitude of the silent phases at $X = 1.0$ indicates that synaptic input for $0 \leq X \leq 0.2$ is severely attenuated by rising stem resistance for $X > 0.2$. **(b)** Periods of high and low potential at the base of the spines are graphed over the same time evolution. The magnitude of the silent phases at $X = 1.0$ demonstrates that synaptic input (in the absence of APs) is severely attenuated by the (fixed) cable input resistance (R_∞). **(c)** State diagrams show the relationship between calcium and stem resistance over the same time period. Behavior is cyclic under synaptic activation (left) as R_{ss} crosses threshold and C_a crosses C_{crit}. Downstream (right), morphology tends to (C_{min}, R_{max}) (long spines with minimal free calcium), due to attenuated activity during silent phases and a persistent rise in stem resistance.

Fig. 6 Closed-curve behavior is persistent for the morphological system under synaptic activation. Additional trajectories are superimposed for the same simulation as in Fig. 5c ($g_p = 0.074\text{n}S$) at $X = 0.0$, varying the initial conditions for calcium and resistance to observe the behavior of the system under synaptic activation. The dark, solid trajectory repeats the simulation from Fig. 5 over 500 activations. The dotted outer trajectory also runs for 500 cycles. The dashed inner trajectory begins near the center of the region and runs for 1200 synaptic activations.

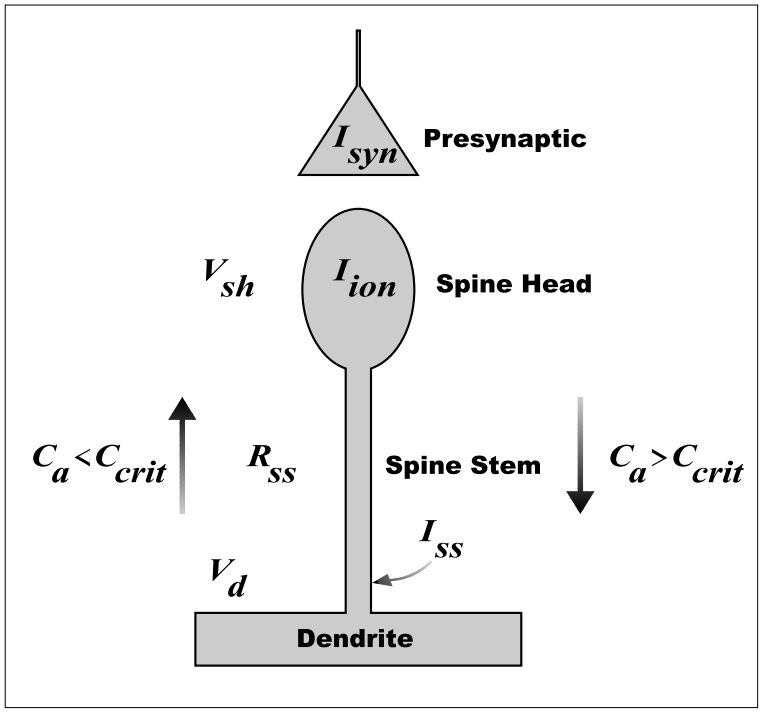
I_{syn}
Presynaptic
V_{sh}
I_{ion}
Spine Head
$C_a < C_{crit}$
R_{ss}
Spine Stem
$C_a > C_{crit}$
I_{ss}
V_d
Dendrite

Figure 1:

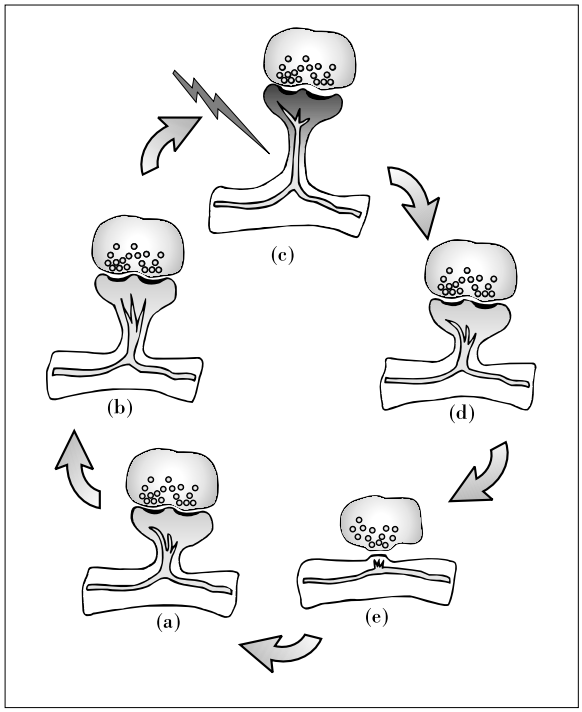

Figure 2:

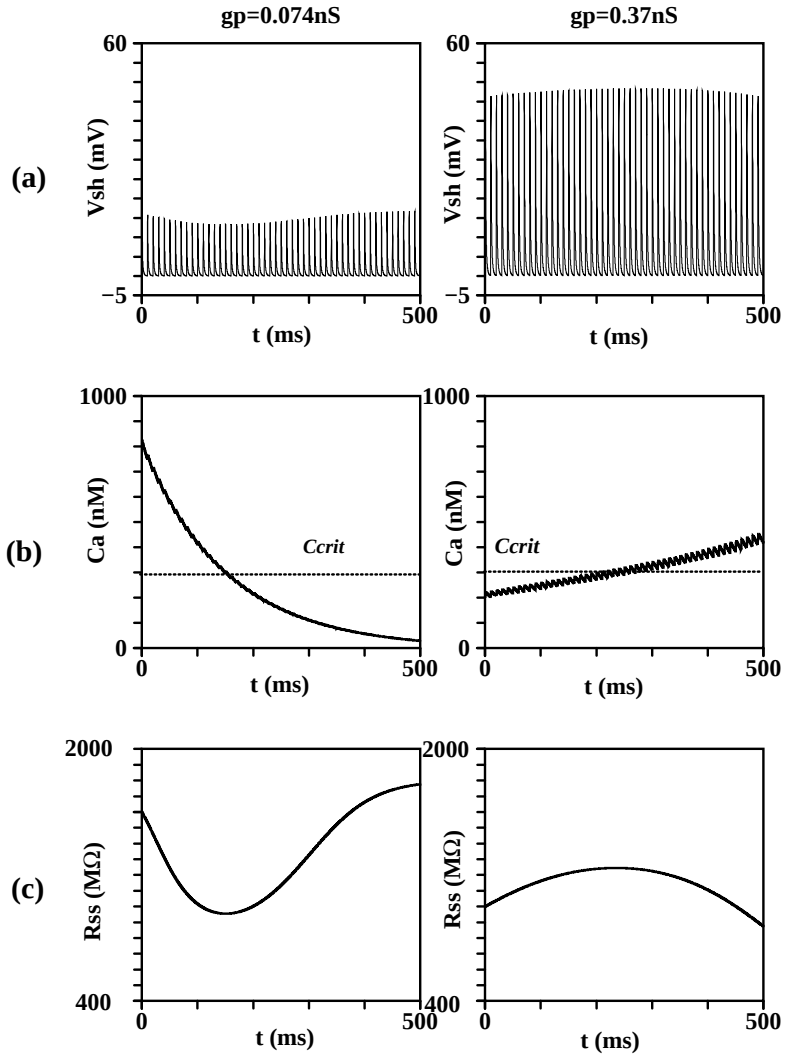
gp=0.074nS
gp=0.37nS
(a)
(b)
(c)
Vsh (mV)
Ca (nM)
Rss (MΩ)
Ccrit
t (ms)
60
−5
1000
0
2000
400
500

Figure 3:

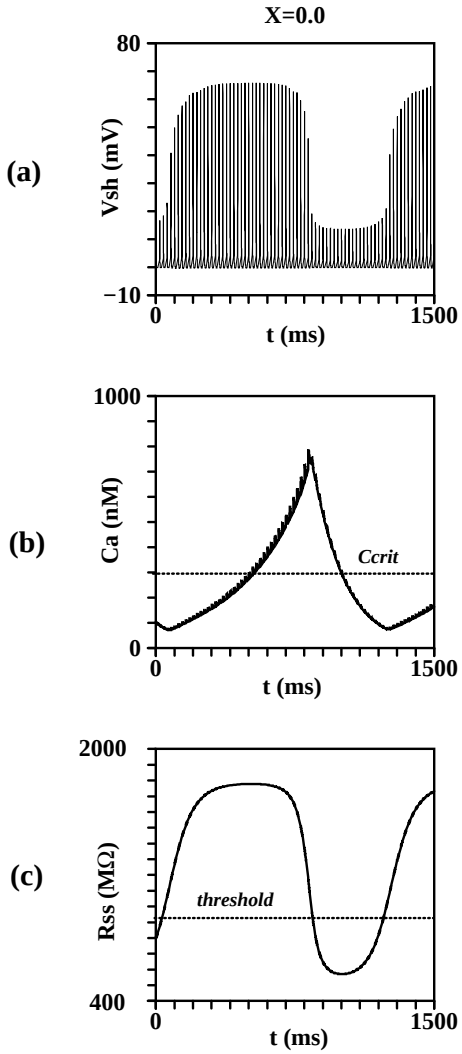
X=0.0
(a)
80
Vsh (mV)
−10
0
1500
t (ms)
(b)
1000
Ca (nM)
Ccrit
0
0
1500
t (ms)
(c)
2000
Rss (MΩ)
threshold
400
0
1500
t (ms)

Figure 4:

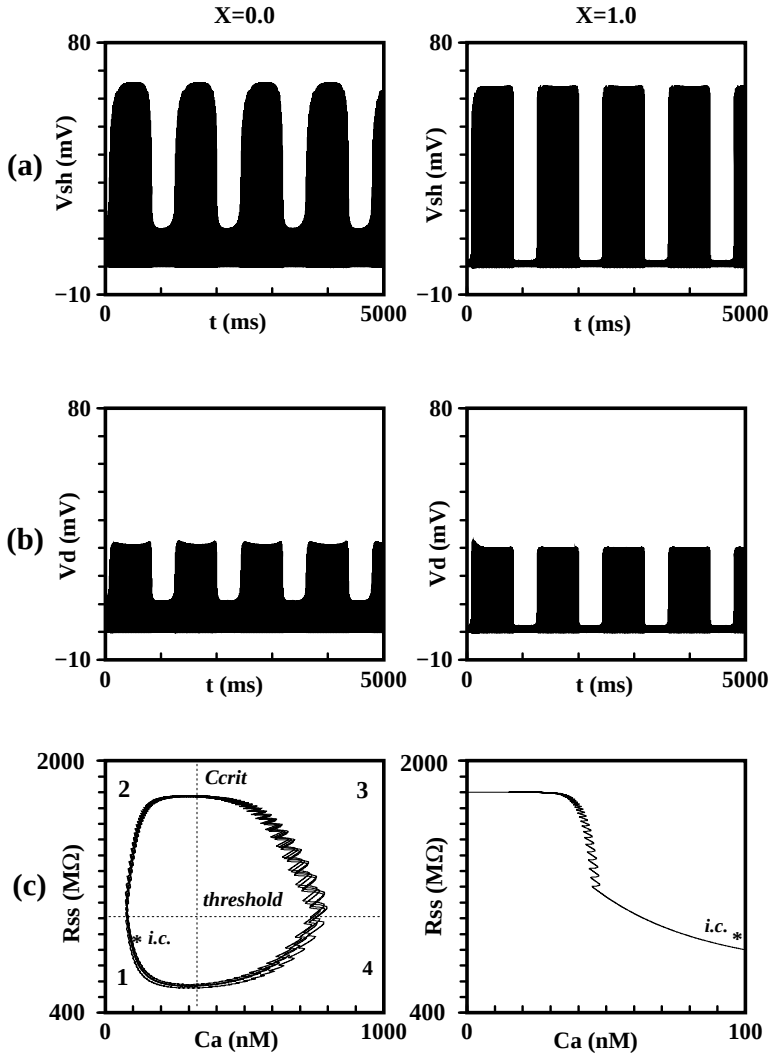
X=0.0
X=1.0
(a)
(b)
(c)
Vsh (mV)
Vd (mV)
Rss (MΩ)
80
−10
0
5000
t (ms)
2000
400
1000
100
Ca (nM)
Ccrit
threshold
i.c.
1
2
3
4

Figure 5:

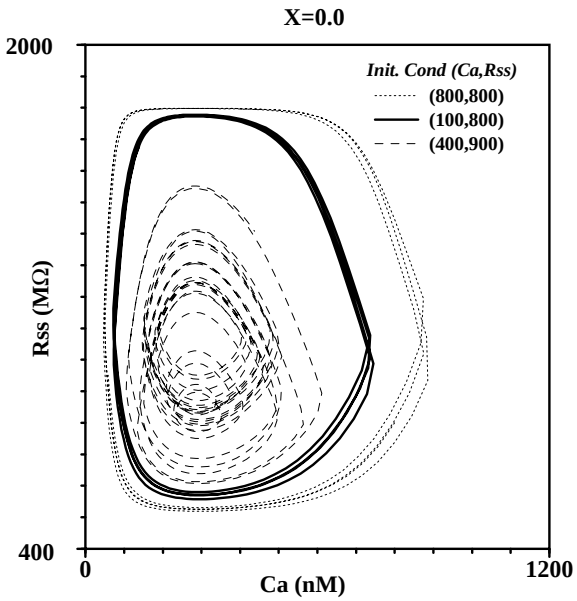
X=0.0
2000
400
0
1200
Rss (MΩ)
Ca (nM)
Init. Cond (Ca,Rss)
(800,800)
(100,800)
(400,900)

Figure 6: